Lithuanian Journal of Physics
Vol. **66**, No. 3, pp. 185–200 (2026)
ISSN 1648-8504 eISSN 2424-3647
DOI: https://doi.org/10.3952/physics.2026.66.3.5

FIRST-PRINCIPLES INVESTIGATION OF THE STRUCTURAL, ELECTRONIC, MAGNETIC AND OPTICAL PROPERTIES OF MAGNETIC SEMICONDUCTING ALLOYS $Zn_{1-x}Ni_xO$ IN THE ZINC-BLENDE, ROCKSALT AND WURTZITE PHASES

F. Redjem [a], K. Souleh [b], H. Mouloudj [c], B. Lagoun [d], H. Lidjici [a], S. Djaili [e], A. Amor [f], and T. Smain [f]

[a] *Laboratoire de matériaux pour Application et Valorisation des Enérgies Renouvelables (LMAVER), Université Amar Telidji, Bp37G 03000 Laghouat, Algeria*
[b] *Laboratoire d'étude et développement des Matériaux Semi-conducteur et Diélectriques (LEDMaScD), Université Amar Telidji, Bp37G 03000 Laghouat, Algeria*
[c] *Laboratoire de Physique des Particules et Physique Statistique, Ecole Normale Superieure-Kouba, P.O. Box 92, Vieux-Kouba, 16050 Algiers, Algeria*
[d] *Materials Physics and Chemistry Laboratory, Amar Telidji University, Laghouat, Algeria*
[e] *Department of Physics, High Teacher's School-Laghouat, 03000, Algeria*
[f] *Faculty of Exact Sciences, Department of Physics, Ziane Achour University, Djelfa, Algeria*
Email: f.redjem@lagh-univ.dz

Received 2 November 2025; revised 13 June 2026; accepted 16 June 2026

In this study, using spin-polarized density functional theory (DFT) calculations, a detailed investigation is conducted into the structural, electronic, magnetic and optical properties of $Zn_{1-x}Ni_xO$ ternary alloys in the wurtzite, zinc-blende and rocksalt crystal phases. The calculated lattice parameters show a a slight non-linear variation with Ni concentration, indicating a minor deviation from Vegard's law in the intermediate composition range. Electronic structure calculations reveal that all investigated alloys preserve their semiconducting nature throughout the entire composition range, although both the type and value of the band gap depend strongly on the crystal phase and Ni content. Charge density analysis suggests that pure ZnO exhibits a partially covalent bonding character, that gradually weakens as the concentration of Ni increases. The magnetic results show that NiO possesses a total magnetic moment of 4 μB per unit cell in the wurtzite phase and 2 μB per unit cell in the zinc-blende and rocksalt phases. Optical investigations indicate that both alloying and phase transitions significantly modify the optical response of the material. Notably, the alloys exhibit a strong absorption over a broad photon energy range, with the rocksalt phase showing the highest absorption. The static refractive indices for various compositions and crystal structures are also reported.

Keywords: structural properties, electronic structure, magnetism, optical spectra, $Zn_{1-x}Ni_xO$ alloys, *ab initio* calculations

1. Introduction

Significant research interest has recently focused on II–VI semiconductor materials for optoelectronic devices that work from blue to near-UV regions [1–5]. The wide band characteristics of these materials, from which they are made, make them very attractive for applications in the high performance blue and UV ranges [6, 7]. Normally, II–VI semiconductors crystallize into either wurtzite (B4) hexagonal or zinc-blende (B3) cubic structures.

Among the direct wide band gap II–VI semiconductors, zinc oxide (ZnO) demonstrates this potential. It is transparent to visible light at room temperature with an energy band gap of 3.37 eV [8] and is characterized by ionicity lying between

covalent and ionic semiconductors [9]. These features are behind its numerous uses as piezoelectric transducers and sensors, in addition to surface acoustic wave devices, but also as transparent conducting oxides, e.g. solar cell electrodes [8–11].

Recently, researchers have shown an increased attention towards dopants such as transition metals (TMs), especially ZnO-based II–VI compounds. This was motivated by the theoretical forecasts of room temperature ferromagnetism in these doped systems making them potential spintronic materials [12].

Given its distinguishing characteristics, including its ferromagnetic nature, exceptional corrosion resistance, and moderately conducting behaviour for both heat and electricity, Ni has been extensively researched as a magnetic impurity among TM elements. Furthermore, due to its near-identical atomic radius and oxidation state to Zn^{2+} [13], Ni^{2+} is regarded as one of the best dopants for ZnO [14–16]. Despite a large number of studies on Ni:ZnO, the experimental and theoretical results are still few or debatable [17–31]. Therefore, more research on $Zn_{1-x}Ni_xO$ is needed to have a better understanding of its basic characteristics. However, in order to create semiconductor-based spintronic devices, a detailed investigation of this material $Zn_{1-x}Ni_xO$ is still necessary in order to find new properties in it.

This study explores the structural, electronic, magnetic and optical properties of of $Zn_{1-x}Ni_xO$ ($0 \le x \le 1$) across three hypothetical phases: zinc-blende (ZB), rocksalt (RS) and wurtzite (WZ). These calculations employ spin-polarized density functional theory (DFT) implemented via the full-potential linearized augmented plane wave (FP-LAPW) method, utilizing the Wu–Cohen generalized gradient approximation (GGA-WC).

2. Computational details

Our computational approach relied on the FP-LAPW method within the framework of DFT [32, 33], as implemented in the Wien2k code [34]. To accurately describe the exchange-correlation potential, we employed the Tran–Blaha modified Becke–Johnson generalized gradient approximation (TB-mBJ-GGA) [35]. All calculations were performed in a spin-polarized framework to account for magnetic effects.

In the method employed, the unit cell is partitioned into distinct muffin-tin (MT) spheres and an interstitial region, ensuring no overlap between the spheres. For all structures, ZB, RS and WZ, the R_{MT} is adopted to be 1.8 Bohr for Zn and Ni atoms and 1.6 Bohr for O atoms. To expand the wave function inside the muffin tin sphere, the maximum value of angular momentum was taken as $l_{max} = 10$. For the wave function, the plane wave cutoff parameter $K_{max} \times R_{MT} = 7$ was used. The space groups are $F_{4-3}m$ (216), Fm_3m (225) and $P6_3mc$ (186) for ZB, RS and WZ structures, respectively. In our calculations, for the integration of Brillouin zone we used 172, 125 and 128 k-points in the irreducible Brillouin zone, for ZB, RS and WZ structures, respectively, and for all concentrations of $Zn_{1-x}Ni_xO$ based on the Monkhorst and Pack scheme [36, 37]. For $Zn_{1-x}Ni_xO$ (x = 0, 0.25, 0.5, 0.75, 1) we constructed the so-called supercell of 1 × 1 × 1 configuration, containing 8 atoms, where we replaced the Zn atom at site 1 by Ni to get the required doping concentration. Structural optimization of the alloyed systems was carried out, with iterations repeated until the total energy convergence criterion of less than 10^{-5} Ry was satisfied.

3. Results and discussion

3.1. Structural properties

In this study, for each doping concentration x, equilibrium lattice parameters were determined by computing the total energy across a series of supercell volumes and fitting the resulting energy–volume curves to the Birch–Murnaghan equation of state [38]. Table 1 presents our result concerning lattice parameters (a and c in the case of WZ structure), for $Zn_{1-x}Ni_xO$ at different Ni contents computed using the Wu–Cohen (WC)-GGA approach [39], alongside comparative experimental and theoretical literature data.

For the lattice parameter a_0, our results agree well with those calculated by Bakhtiar Ul Haq et al. [40, 41] for all concentrations of ZB $Zn_{1-x}Ni_xO$. According to Ref. [40], we only have experimental data for the ZB structure of $Zn_{1-x}Ni_xO$ when $x = 0$, which means that it is pure ZnO. The lattice parameter that we calculated is a little different from the experimental value given in that reference. For the RS structure, our result for ZnO ($x = 0$) matches up very well with the experimental measurement that Özgür et al. [42] did, using X-ray diffraction.

Table 1. Calculated lattice parameters of three phases of $Zn_{1-x}Ni_xO$ (x = 0, 0.25, 0.5, 0.75, 1).

Parameter/material	ZnO	$Zn_{0.75}Ni_{0.25}O$	$Zn_{0.5}Ni_{0.5}O$	$Zn_{0.25}Ni_{0.75}O$	NiO
ZB					
a_0 (Å)	4.55[a]	4.53[a]	4.50[a]	4.46[a]	4.41[a]
	4.55[b]	4.60[d]	4.54[d]	4.50[d]	
	4.60[c]				
RS					
a_0 (Å)	4.27[a]	4.23[a]	4.19[a]	4.16[a]	4.13[a]
	4.271[e]				4.17[f]
WZ					
a_0 (Å)	3.22[a]	3.21[a]	3.19[a]	3.16[a]	3.09[a]
	3.2495[g]				
c_0 (Å)	5.26[a]	5.24[a]	5.19[a]	5.16[a]	5.21[a]
	5.2069[g]				

[a] This work.
[b] Calc. Ref.40].
[c] Exp. quoted in Ref.40].
[d] Calc. Ref.41].
[e] Exp. Ref.42].
[f] Exp. Ref.43].
[g] Exp. quoted in Ref.44].

However, for NiO (x = 1), our calculated lattice parameter a_0 is slightly lower than the experimental value reported by Benzerouk (4.17 Å) using X-ray diffraction measurements [43]. For the WZ structure, our calculated values for a_0 and c_0 in ZnO (x = 0) are less than 1 and 2% different from the experimental data in Ref. [44], respectively. Since there is no experimental or theoretical data for intermediate concentrations ($0.25 \leq x \leq 1$) in the RS structure or for a_0 and c_0 in the WZ structure, our results in these cases are just theoretical predictions. Figure 1 displays the variation of lattice parameters as a function of Ni concentration x in $Zn_{1-x}Ni_xO$ for all studied phases: ZB, Fig. 1(a); RS, Fig. 1(b); WZ, Fig. 1(c). The lattice parameter a exhibits a progressive decrease with increasing x from ZnO (x = 0) to NiO (x = 1) in both cubic phases ZB and RS, Fig. 1(a, b). A similar trend is observed for the lattice parameters a_0 and c_0 in the case of the WZ structure, Fig. 1(c). Across all structures, lattice parameters vary nonlinearly yet monotonically. This systematic deviation from Vegard's linear law [45] aligns with the reported violations in other semiconductor alloys [46–52].

3.2. Electronic properties

As reference systems, the electronic band structures of the end-member compounds ZnO (x = 0) and NiO (x = 1) in the ZB, RS and WZ phases were calculated using the TB-mBJ-GGA approach [35]. ZnO exhibits semiconducting behaviour in all phases, with the WZ phase showing a direct band gap of 2.83 eV at Γ, slightly underestimated relative to the experiment, as commonly observed in semi-local DFT methods [9, 35, 60]. The ZB and RS phases also remain semiconducting, in agreement with previous theoretical studies [11, 53–57]. In contrast, NiO shows a strongly spin-polarized electronic structure dominated by Ni-3d and O-2p hybridized states near the Fermi level, reflecting its correlated nature [27, 30, 43]. These results establish the electronic characteristics of the parent compounds and provide a reference for analyzing the evolution of the electronic structure in $Zn_{1-x}Ni_xO$ alloys.

In this study, the electronic band structures of $Zn_{1-x}Ni_{1-x}O$ alloys were calculated for the hypothetical ZB, RS and WZ phases, across various Ni concentrations x = 0, 0.25, 0.5, 0.75, 1 using the TB-mBJ-GGA method. For magnetic systems, including the NiO compound and Ni-containing alloys, spin polarization was taken into account. Given the overall similarity in the band structure profiles across the different compositions, we focus on presenting the results for the equimolar alloy $Zn_{0.50}Ni_{0.50}O$ in all three crystal structures, for both spin-up and spin-down channels. These results are depicted in Fig. 2.

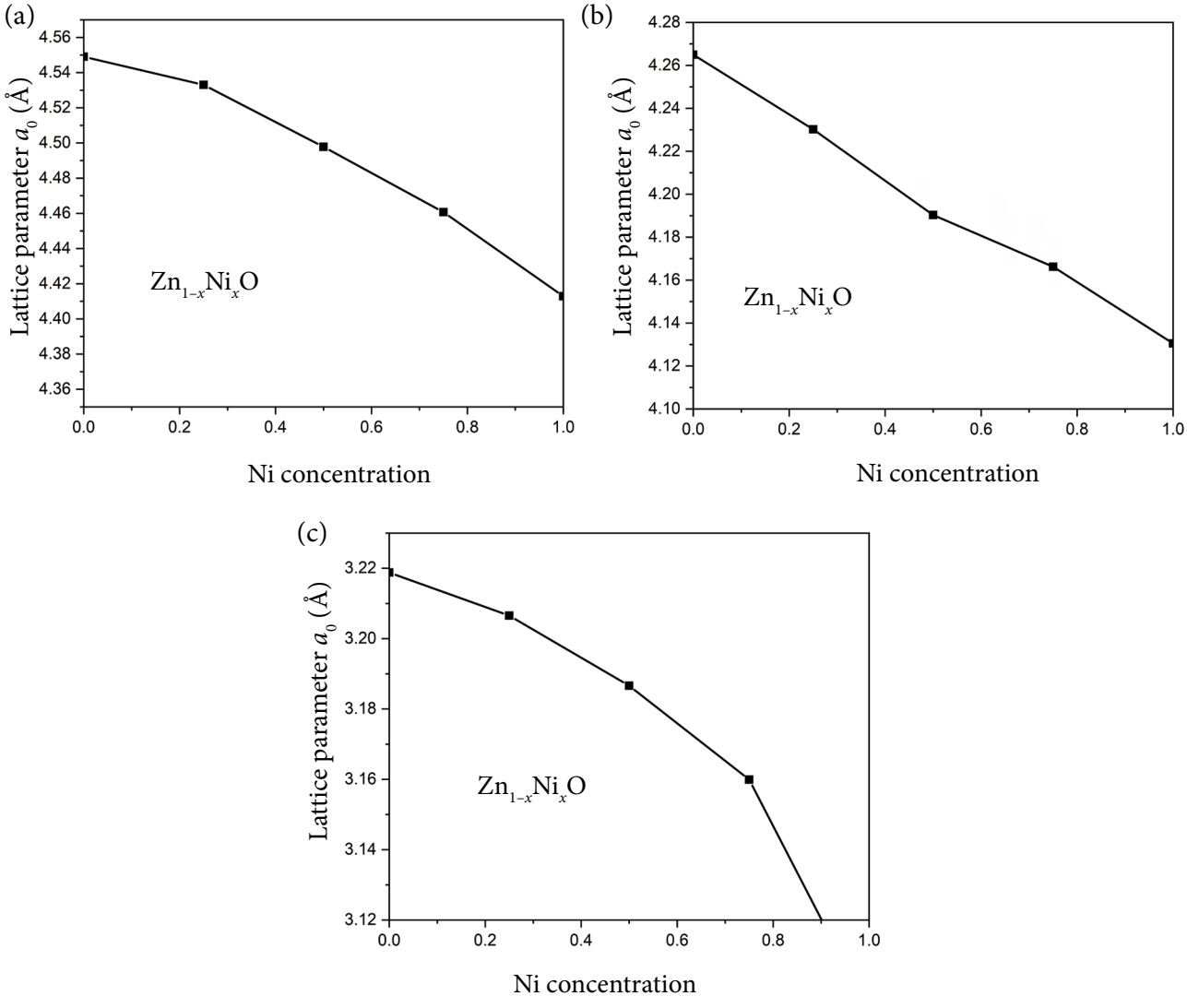

Fig. 1. (a) Lattice parameter a_0 versus Ni concentration in ZB $Zn_{1-x}Ni_xO$. (b) Lattice parameter a_0 versus Ni concentration in RS $Zn_{1-x}Ni_xO$. (c) Lattice parameters a_0 and c_0 versus Ni concentration in WZ $Zn_{1-x}Ni_xO$.

Qualitatively, the band structures exhibit comparable features across the three structural phases, closely resembling the trends observed in prior studies of semiconducting materials [53–57]. However, quantitative differences emerge in the values of the band gap energies. A detailed examination reveals that for the spin-up channel, $Zn_{0.50}Ni_{0.50}O$ exhibits a direct band gap of 2.16 eV at the (Γ → Γ) point in the ZB structure, an indirect band gap of 2.92 eV (from R to Γ) in the RS phase, and a direct band gap of 1.63 eV at the (Γ → Γ) point in the WZ structure.

The electronic band structures over the full composition range $Zn_{1-x}Ni_xO$ alloys ($0 \le x \le 1$) were calculated for three hypothetical crystal phases ZB, RS and WZ, and used to determine the fundamental band gap energy (E_g). The dependence of Eg on Ni concentration is summarized in Table 2 and illustrated in Fig. 3.

For the ZB structure, E_g exhibits an overall decreasing trend with increasing Ni concentration, with a slight deviation from linearity at intermediate compositions. The band gap undergoes a pronounced redshift from approximately 3.15 eV for pure ZnO ($x = 0$) to about 0.78 eV for NiO ($x = 1$). In the RS phase, E_g shows a generally increasing trend with Ni incorporation, evolving from 3.12 eV for ZnO to 3.66 eV for NiO. Minor deviations from linear behaviour are observed at intermediate concentrations, but the overall dependence remains monotonic.

Similarly, for the WZ structure, the band gap decreases overall with increasing Ni content, from 2.86 eV for pure ZnO to 1.81 eV for NiO, with small departures from linearity at selected compositions.

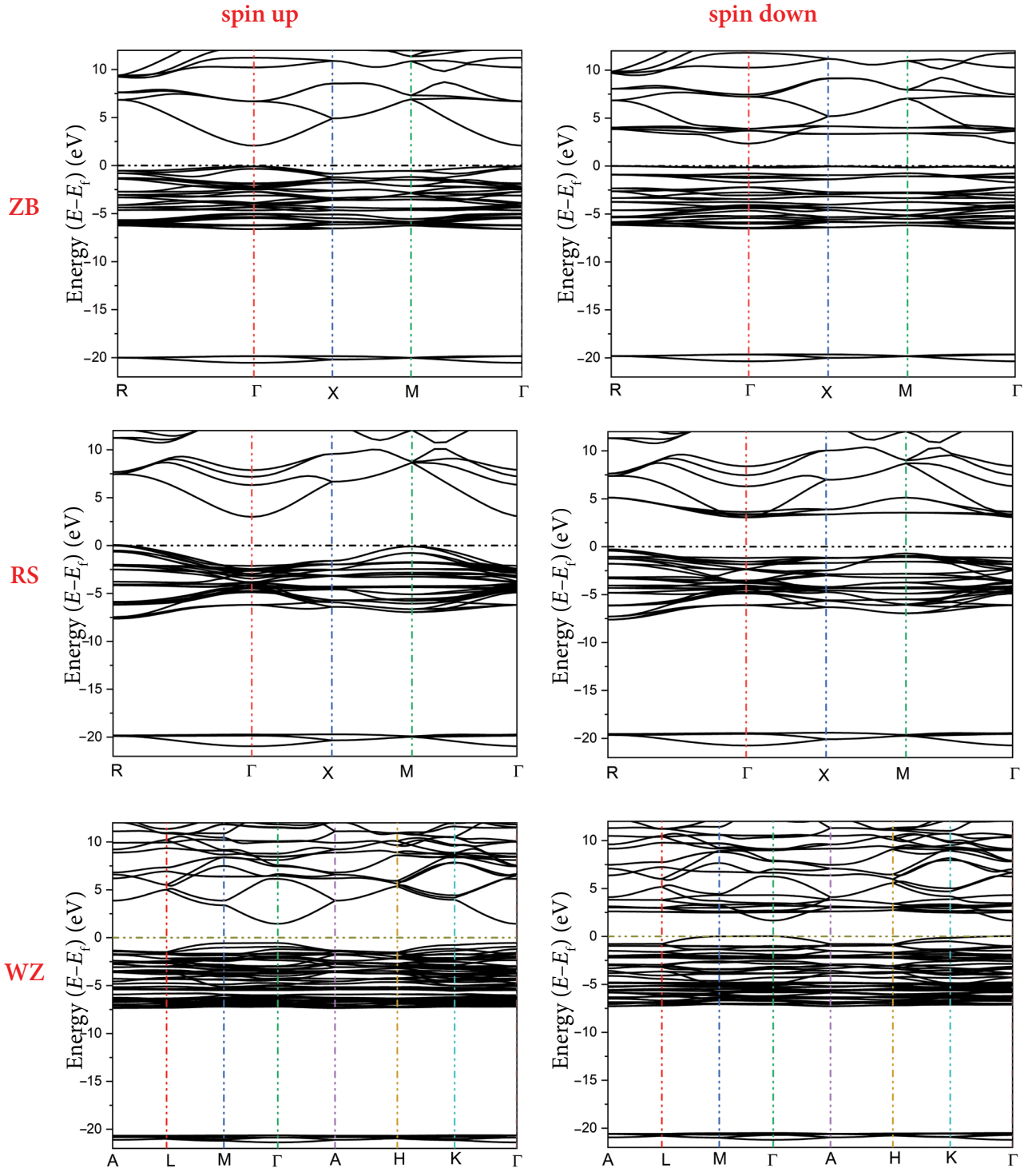

Fig. 2. Electronic band structure for $Zn_{0.50}Ni_{0.50}O$ in the ZB, RS and WZ structures, considering both spin channels.

These results indicate that Ni substitution induces a systematic modification of the electronic structure across all phases, leading to band gap narrowing or widening depending on the crystal structure.

Our calculations, performed at room temperature and ambient pressure, yield a band gap E_g of 2.83 eV for wurtzite ZnO. While this value underestimates the experimental result of 3.23 eV [58], it compares favourably with the recent computational value of 2.77 eV obtained using a similar methodology [59]. The remaining difference between the calculated and experimental band gap originates from the approximate nature of the mBJ potential [60]. Consequently, the calculated E_g

Table 2. Evolution of the fundamental band-gap energy E_g as a function of Ni content for ZB, RS and WZ hypothetical structures of $Zn_{1-x}Ni_xO$.

	ZnO	$Zn_{0.75}Ni_{0.25}O$	$Zn_{0.5}Ni_{0.5}O$	$Zn_{0.25}Ni_{0.75}O$	NiO
ZB					
E_g (Γ → Γ) (eV)	2.65	1.89	2.16	2.07	1.87
RS					
E_g (R → Γ) (eV)	3.12	2.65	2.92	3.21	3.66
WZ	2.83				
E_g (Γ → Γ) (eV)	3.23[a]	2.43	1.63	2.29	1.81
	2.77[b]				

[a] Exp. Ref.58].
[b] Calc. Ref.59].

values for the other structures are also expected to be underestimated relative to the experiment.

The density of states (DOS) for $Zn_{1-x}Ni_xO$ alloys with compositions x = 0, 0.25, 0.5, 0.75, 1 has been computed for the three hypothetical crystal structures ZB, RS and WZ to gain deeper insight into the electronic distribution among various atomic orbitals. Representative DOS results for ZnO, the equimolar alloy $Zn_{0.50}Ni_{0.50}O$ and NiO are presented in Fig. 4. A detailed analysis of the ZB phase reveals that the states near the Fermi level in pure ZnO are primarily dominated by Zn 3d orbitals.

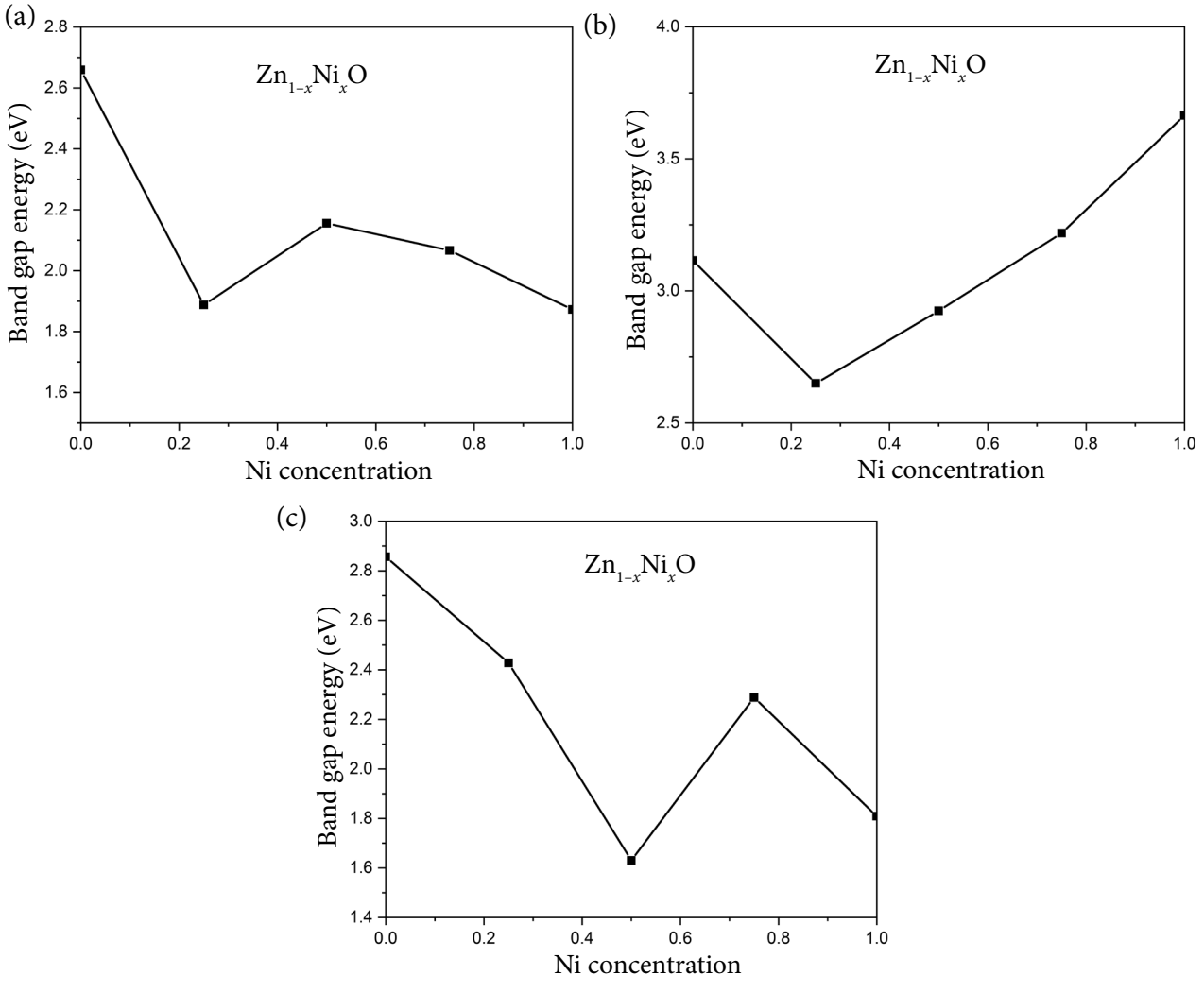

Fig. 3. Fundamental band gap energy versus Ni content in (a) the ZB structure, (b) the RS structure and (c) the WZ structure for the spin up channel.

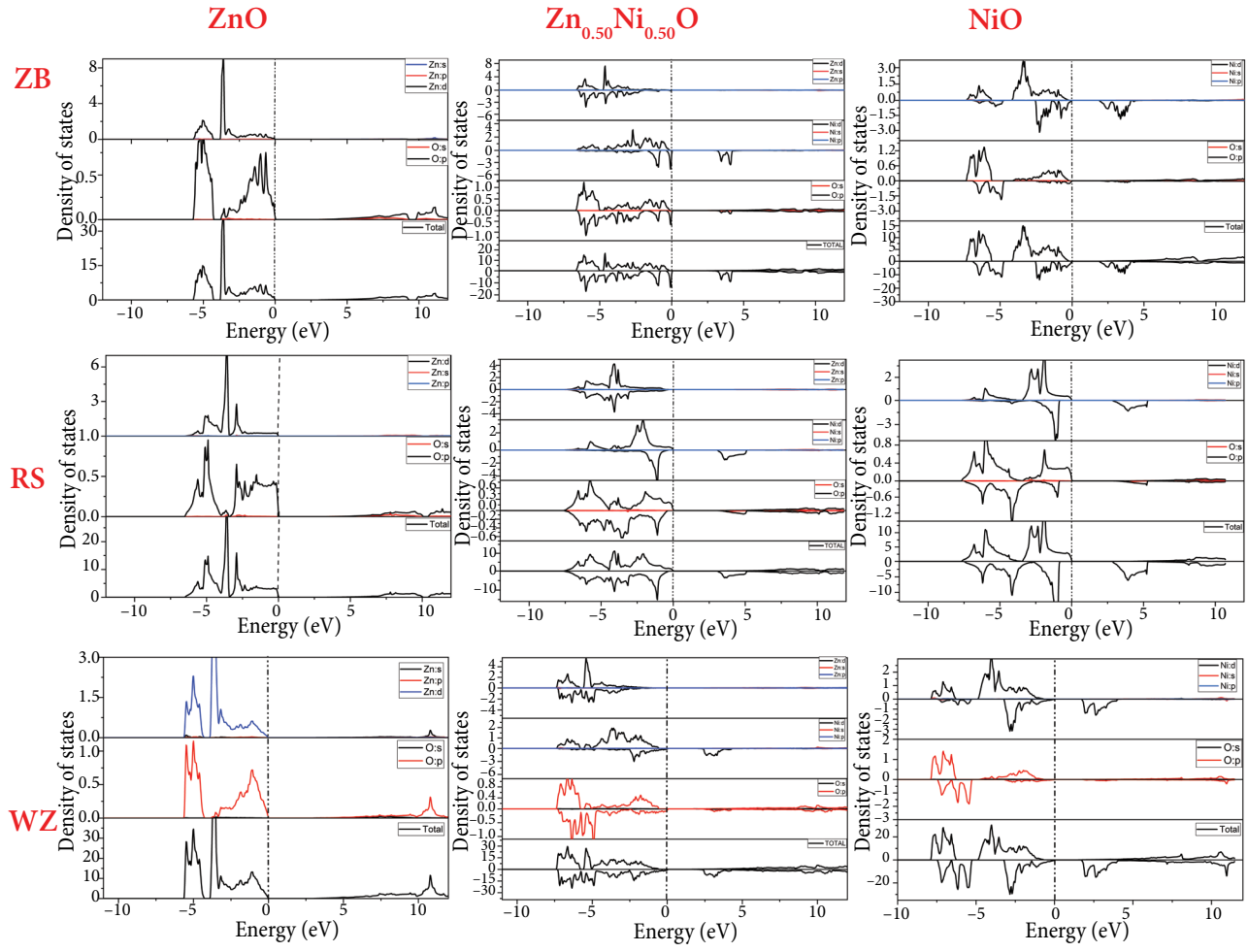

Fig. 4. Density of states of ZnO, $Zn_{0.50}Ni_{0.50}O$ and NiO in the ZB, RS and WZ structures, considering both spin channels.

This trend is consistently observed in both the RS and WZ phases of ZnO, confirming the crucial role of Zn-d states in the electronic conductivity of the material across all structural forms. In these energy regions, the total DOS is mainly composed of Zn-d and O-2p states. Among them, the WZ phase exhibits the most tightly bound lower energy band in its DOS. For the $Zn_{0.50}Ni_{0.50}O$ alloy, the electronic states near the Fermi level are primarily contributed by the d orbitals of both Zn and Ni atoms, along with the p orbitals of oxygen. This orbital configuration remains consistent across all three structures, emphasizing the hybridized nature of metal-d and O-p states in Ni-doped ZnO.

Understanding the electronic charge density in semiconducting materials is of great significance as it provides important information about the nature of chemical bonding, the presence of interstitial impurities, and how the material reacts to outside forces [61–64]. We have figured out the charge densities of the valence electrons in $Zn_{1-x}Ni_xO$ alloys with different compositions (x = 0, 0.25, 0.5, 0.75, 1) and three different crystal structures: ZB, RS and WZ.

Figure 5 shows example charge density contour plots for compositions x = 0, 0.50 and 1 in all three phases. The contours show that for pure ZnO (x = 0), the electronic charge is mostly concentrated in the spaces between atoms and is clearly tilted towards the oxygen atoms. This uneven charge distribution shows that a lot of charge has moved from the group II element (Zn) to the group VI element (O). This confirms that the Zn–O bond is mostly ionic. The lower-energy valence bands have s-like orbital features, and the mid-gap states seem to have some covalent character, even though there is not much electronic density in the spaces between the atoms.

The charge buildup around the oxygen atoms becomes stronger as the Ni content rises, like in the equiatomic alloy $Zn_{0.50}Ni_{0.50}O$. This increased

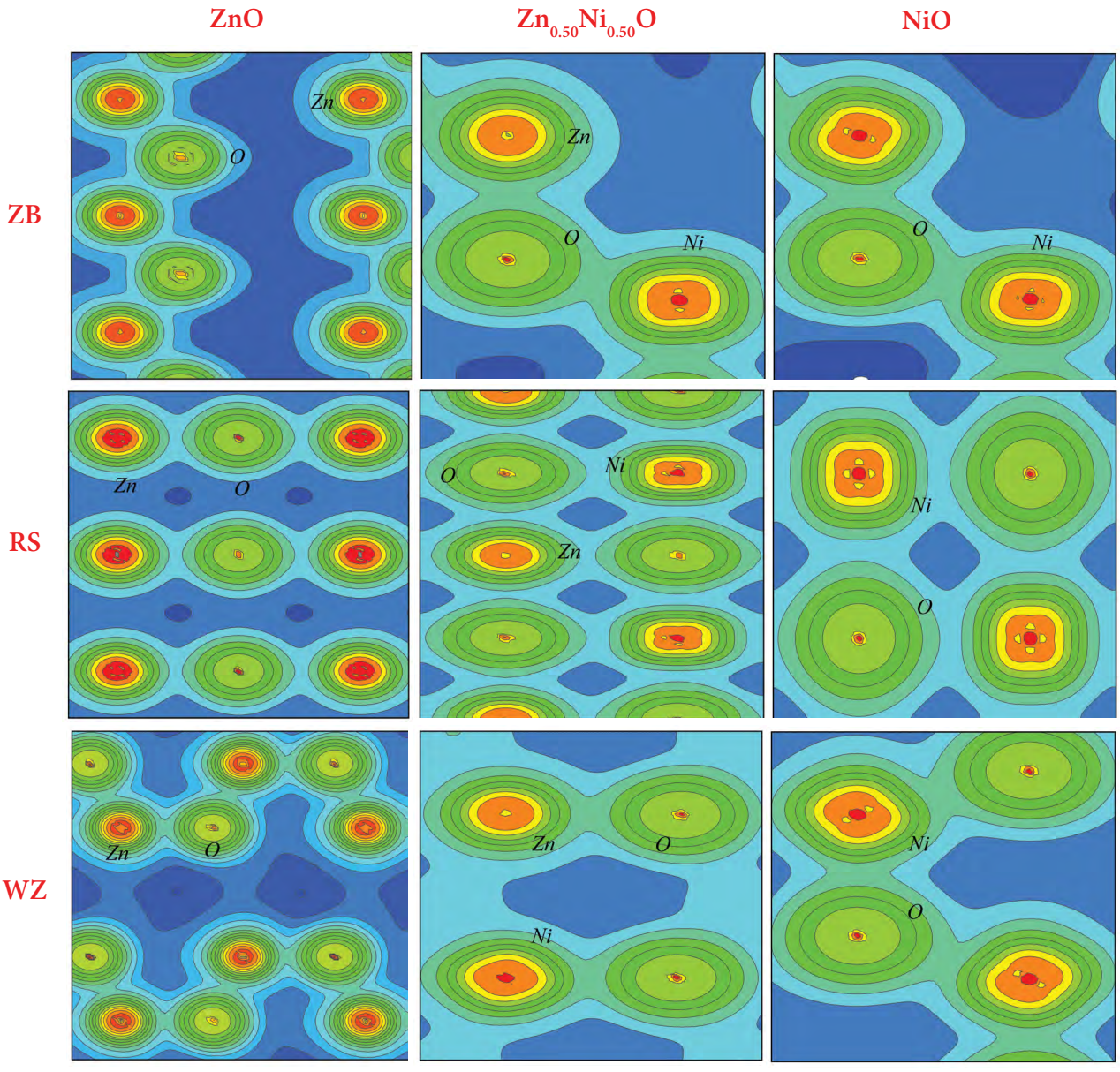

Fig. 5. Electronic valence charge density (contour plots) of ZnO, $Zn_{0.50}Ni_{0.50}O$ and NiO in the ZB, RS and WZ structures for the spin up channel.

polarization makes the ionic nature of the bonding in the alloy even stronger, more than what is seen in pure ZnO. At the Ni-rich end of the series (x = 1), the charge density of NiO shows that the Ni–O bonds are very ionic.

In general, the charge density maps for the ZB and RS phases show similar patterns, but there are small differences in the way the charges are spread out. On the other hand, the WZ structure shows a more clear charge localization behaviour, which shows how crystallographic symmetry affects the way bonds form. These findings show that the way electronic charge is spread out and how bonds form in $Zn_{1-x}Ni_xO$ alloys depends on their structure.

3.3. *Magnetic properties*

We have carefully calculated the total magnetic moment of $Zn_{1-x}Ni_xO$ for all three structural phases that we looked at in this study: ZB, RS and WZ. The range of compositions that we looked at was x = 0 to 1. Figure 6 shows how the total magnetic moment changes with the amount of Ni. Across all structural phases, the total magnetic moment clearly increases in a monotonic but nonlinear way as the concentration of Ni rises. The total magnetic moment in the fully substituted compound NiO (x = 1) is 2, 2 and 4 μ_B per unit cell for the ZB, RS and WZ structures, respectively. For the equiatomic alloy $Zn_{0.50}Ni_{0.50}O$,

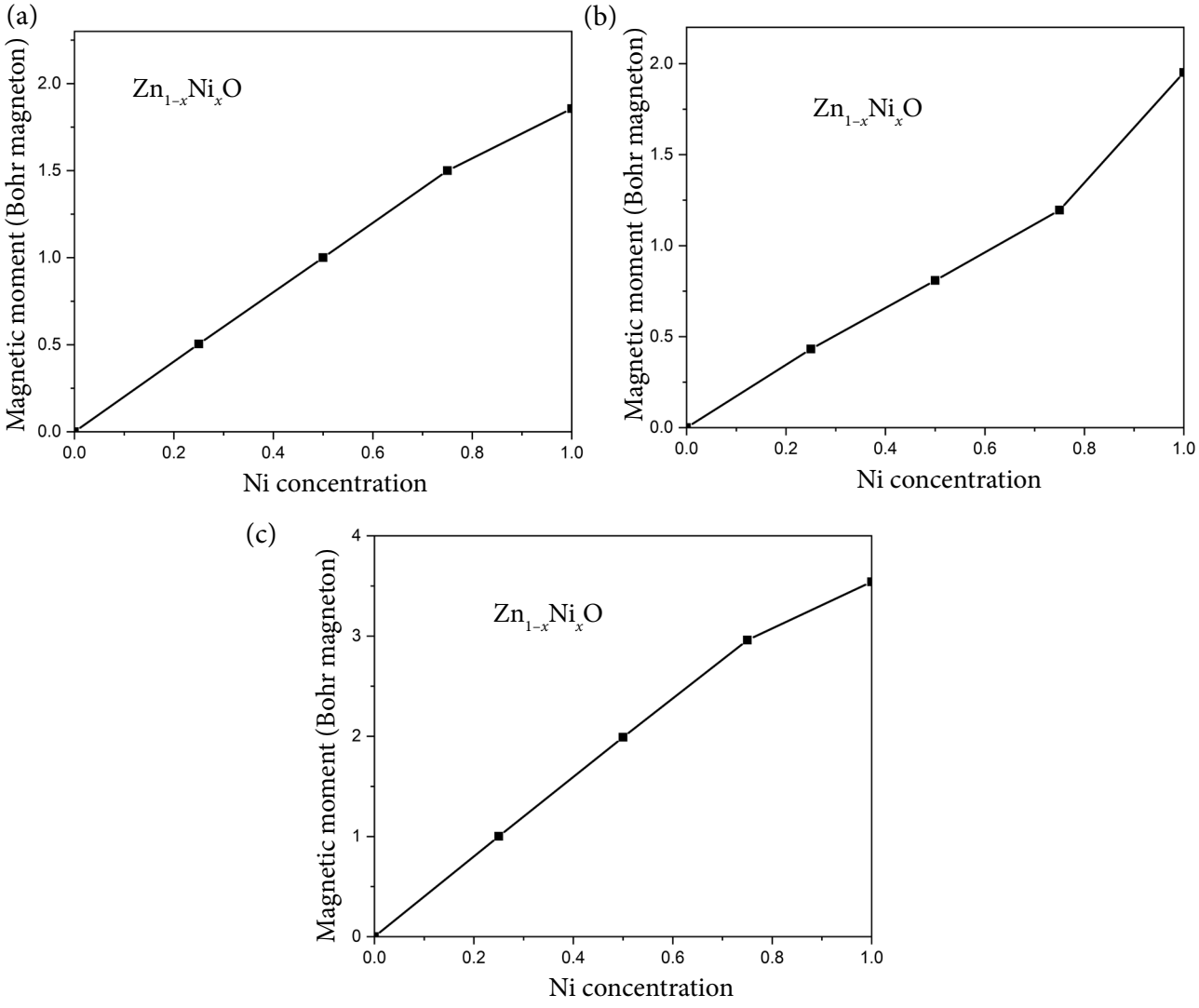

Fig. 6. Total magnetic moment versus Ni content in (a) the ZB structure, (b) the RS structure and (c) the WZ structure.

the values are 1 μ_B for ZB and RS, and 2 μ_B for WZ. These results show that the magnetic response depends a lot on both the composition and the crystal structure. The localized magnetic moments of Ni^{2+} ions in these alloys cause magnetism. These moments come from unpaired electrons in the partially filled 3d orbitals. As a result, the magnetic properties of ZnO alloys with Ni are determined by how these localized d-electrons are spread out and how they interact with each other. NiO has a strong magnetic ordering because Ni^{2+} atomic moments are the most important factor.

3.4. Optical properties

Before presenting the results, it should be noted that the calculation of optical properties requires a denser k-point mesh than that used for structural and electronic property calculations. We used 500, 216 and 432 *k*-points in the first Brillouin zone for the ZB, RS and WZ structures, respectively.

The calculated spectra of the real (ε_1) and imaginary (ε_2) parts of the dielectric function obtained in this study for $Zn_{1-x}Ni_xO$ (x = 0, 0.50, 1) with ZB, RS and WZ structures are displayed in Fig. 7. In the ZB structure with x = 0 (pure ZnO), we see that the real part of the dielectric function ε_1 goes up as the photon energy goes up, reaching a peak around 3.5 eV in the low-photon energy range. After this point, it shows a series of small peaks before dropping quickly to a minimum around 16.5 eV. After this low point, ε_1 goes up again and reaches its highest point at about 27.5 eV.

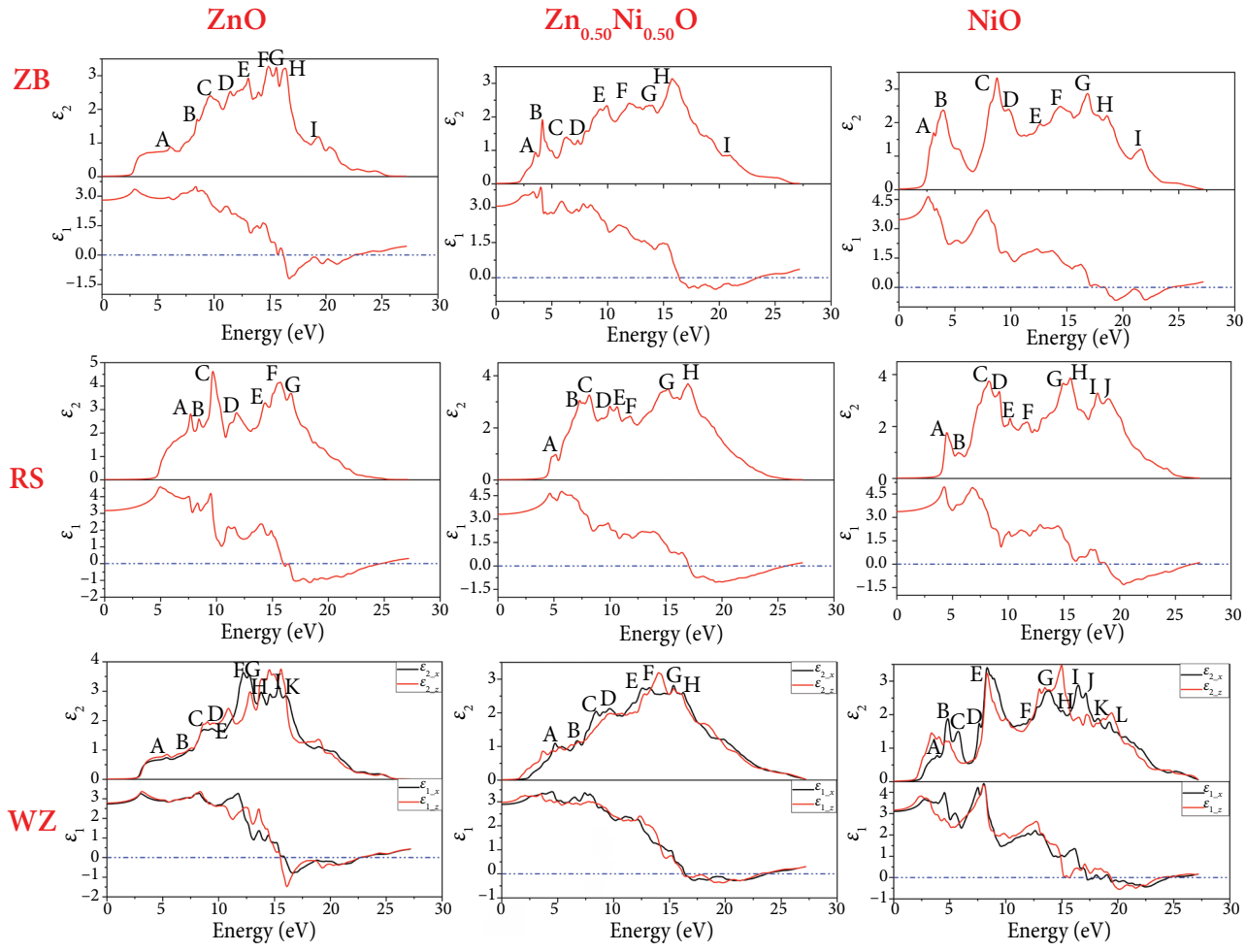

Fig. 7. Real (ε_1) and imaginary (ε_2) parts of the dielectric function spectra for ZB, RS and WZ $Zn_{1-x}Ni_xO$ at Ni concentrations of 0, 0.50 and 1.

The peaks that come after the main maximum are mostly due to interband optical transitions. Khan and Bouarissa [65] used first-principles molecular dynamics simulations to find a qualitatively similar trend for ε_1 as a function of photon energy for the ZnS compound. ε_1 gets closer and closer to the static dielectric constant $\varepsilon(0)$ in the low-energy region, below the reststrahlen band. We found that $\varepsilon(0)$ for ZB ZnO is about 2.9, which is close to the value of 3.27 that Zerroug et al. [51] found.

The imaginary part of the dielectric function ε_2 exhibits a noticeable rise beyond the absorption edge energy. It reaches its first optical critical point ((a) in Fig. 7) at about 7 eV. This rise is the start of direct interband transitions. After point *A*, there are a number of peaks that follow. These peaks are caused by a sudden rise in the number of available transitions that contribute to ε_2. Bouarissa [67] has also reported that the InP compound behaves in a similar way.

The transition from pure ZnO to the equimolar alloy $Zn_{0.50}Ni_{0.50}O$ and finally to pure NiO in the zinc blende (ZB) structure shows that the overall shapes of the real (ε_1) and imaginary (ε_2) parts of the complex dielectric function stay mostly the same. However, there are clear spectral shifts: ε_1 moves towards higher photon energies, while ε_2 moves towards lower energies. These changes in the spectrum have a measurable effect on both parts of the dielectric function, especially the static dielectric constant $\varepsilon(0)$.

In the ZB structure, our calculations show that the static dielectric constant $\varepsilon(0)$ goes from about 3.04 for $Zn_{0.50}Ni_{0.50}O$ to 3.48 for NiO. We do not have any experimental or theoretical data for $\varepsilon(0)$ in $Zn_{0.50}Ni_{0.50}O$ or the ZB-phase NiO, so these values are just guesses.

Across the ZnO–NiO alloy series, the dielectric function shows similar qualitative trends for the RS and WZ phases (see Fig. 7). the ε_1 peak maxima

and critical points in ε_2, on the other hand, are in different places than they are in the ZB structure. These differences in the spectra suggest that the RS and WZ phases may have different optical properties than the ZB phases.

The computed static dielectric constants $\varepsilon(0)$ for the RS phase are about 3.20 for ZnO, 3.32 for $Zn_{0.50}Ni_{0.50}O$ and 3.40 for NiO. When looking at the WZ structure, the $\varepsilon(0)$ values are a little lower, at about 2.7, 2.9 and 3.1. These results show even more than the dielectric response in $Zn_{1-x}Ni_xO$ alloys depends on their structure.

The absorption coefficient $\alpha(\omega)$ is one of the key optical parameters that plays a crucial role in the design and fabrication of optoelectronic devices, reflectivity $R(\omega)$, electron energy loss $L(\omega)$ and refractive index $n(\omega)$ [67–72]. The ZB, RS and WZ phases of ZnO, $Zn_{0.50}Ni_{0.50}O$ and NiO materials $n(\omega)$, $L(\omega)$, $R(\omega)$ and $\alpha(\omega)$ spectra are displayed in Fig. 8. Examining ZB ZnO reveals that $n(\omega)$ has significant values in the low photon energy region and rapidly drops at high photon energy up to 27.5 eV. Based on the $n(\omega)$ spectrum, the static refractive index $n(0)$ for ZB ZnO is estimated to be 1.67.

The $n(\omega)$ spectrum shows a number of small peaks that are thought to be caused by excitonic transitions. The oscillator strength is known to be increased by these excitonic effects, especially at the Brillouin zone's M_0 and M_1 critical points [73, 74]. There are clear peaks in the ZB ZnO $L(\omega)$ spectrum, which are indicative of plasma resonances. The plasma frequency is the associated frequency, and in this instance, it is found to be around 22.5 eV, which corresponds to the loss function's primary peak.

There are multiple prominent peaks in the $R(\omega)$ spectrum, especially in the high-photon-energy region. The valence and conduction bands' inter-

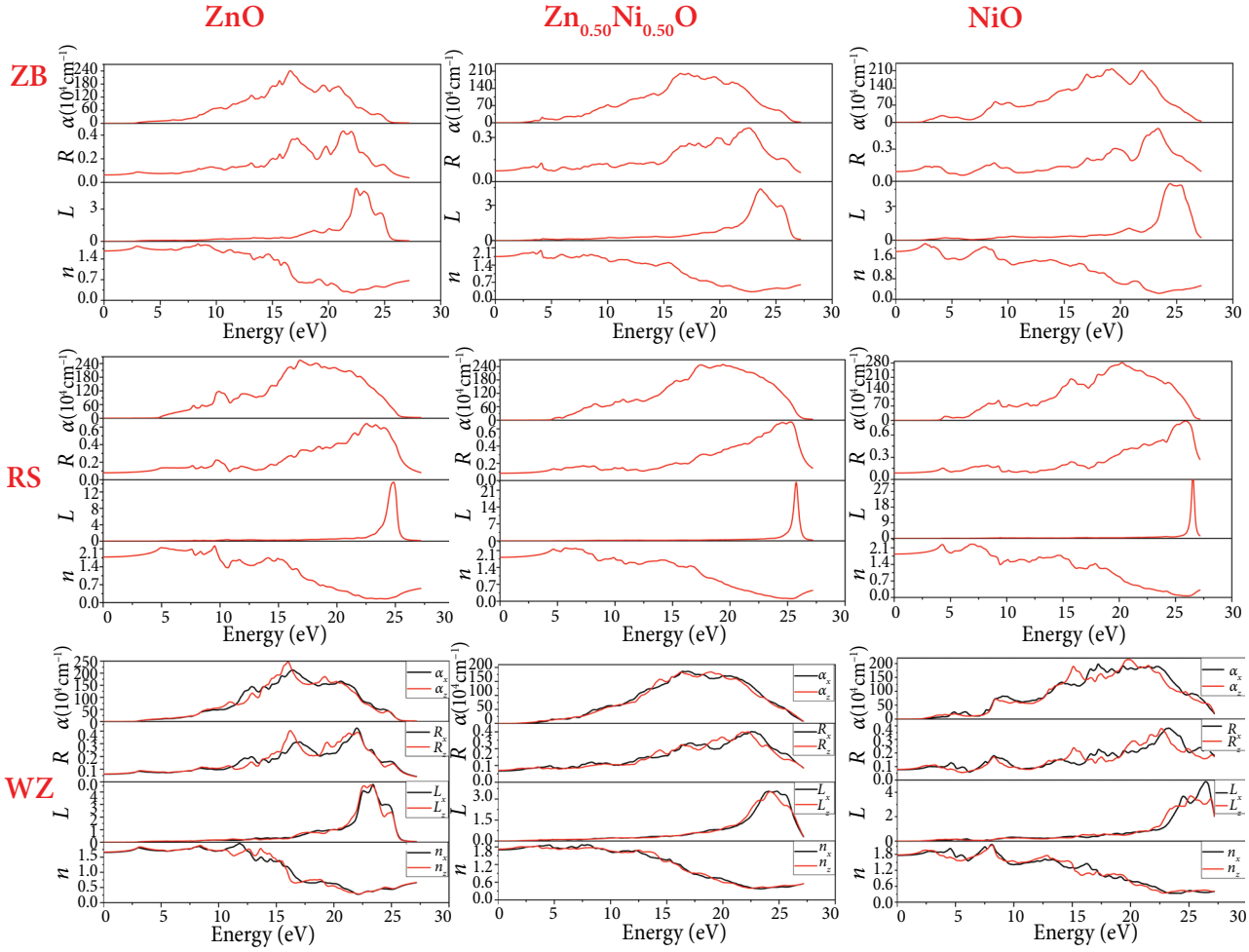

Fig. 8. Refractive index $n(\omega)$, electron energy loss $L(\omega)$, reflectivity $R(\omega)$ and absorption coefficient $\alpha(\omega)$ spectra for ZB, RS and WZ $Zn_{1-x}Ni_xO$ at Ni concentrations of 0, 0.50 and 1.

band transitions are represented by these characteristics. The main cause of these peaks' broadening is phonon–phonon scattering, which causes vibrational damping in the substance. ZB ZnO's absorption coefficient spectrum $\alpha(\omega)$ exhibits a broad absorption band that spans the energy range of 7–27.5 eV, with a noticeable maximum at about 17 eV. The absorption drastically drops at photon energies higher than 27.5 eV, suggesting that the material turns transparent in this high-energy region because the electrons can no longer react to the oscillating electric field efficiently. The general profiles of the optical spectra, which include the absorption coefficient $\alpha(\omega)$, energy loss function $L(\omega)$, reflectivity $R(\omega)$ and refractive index $n(\omega)$, maintain a relatively similar shape as the composition changes from ZB ZnO to ZB $Zn_{0.50}Ni_{0.50}O$ and finally to ZB NiO. Nevertheless, there is a discernible shift towards higher photon energies in all of these spectra. Throughout the energy range, this spectral shift has a major impact on the optical features' position and magnitude. In particular, it is discovered that the static refractive index $n(0)$ rises as the Ni content increases, moving from 1.67 for ZnO to roughly 1.74 for $Zn_{0.50}Ni_{0.50}O$ and 1.86 for NiO. Future theoretical and experimental studies on the optical characteristics of $Zn_{1-x}Ni_xO$ alloys may find these theoretical predictions to be helpful benchmarks and valuable reference points.

The general spectral shapes of $n(\omega)$, $L(\omega)$, $R(\omega)$ and $\alpha(\omega)$ for the RS and WZ structures (Fig. 8) are comparable to those found in the ZB phases of ZnO, $Zn_{0.50}Ni_{0.50}O$ and NiO. Nonetheless, there are minor structural differences in the static refractive index $n(0)$: for the RS phase, the corresponding values for $n(0)$ are 1.78, 1.82 and 1.85 for ZnO, $Zn_{0.50}Ni_{0.50}O$ and NiO, respectively; for the WZ phase, they are 1.67, 1.68 and 1.79.

The primary peaks for the RS and WZ phases of ZnO are situated at roughly 25 and 23 eV, respectively, in the electron energy loss spectrum $L(\omega)$, suggesting a different plasma resonance behaviour. The RS phase of ZnO exhibits a prominent peak at 7.23 eV in its reflectivity spectrum $R(\omega)$, whereas the WZ phase shows peaks at approximately 17 and 22 eV. Regarding the absorption coefficient $\alpha(\omega)$, ZnO's RS and WZ phases both display absorption bands that range in a wavelength from roughly 5 to 26 eV. In contrast to the ZB and WZ phases, the RS structure exhibits a notably higher absorption intensity, indicating an improved light–matter interaction in this phase. Comparing $n(\omega)$, $L(\omega)$, $R(\omega)$ and $\alpha(\omega)$ among ZB, RS and WZ structures shows that the RS phase consistently shows stronger optical responses, with similar trends seen for $Zn_{0.50}Ni_{0.50}O$ and NiO.

4. Conclusions

Within the framework of spin-polarized density functional theory (DFT) using the generalized gradient approximation (GGA), we employed the FP-LAPW method to perform total energy calculations, and the electronic band structure, structural, magnetic and optical properties of Ni-doped ZnO ($Zn_{1-x}Ni_xO$) were examined. For different compositions, the hypothetical phases of WZ, RS and ZB were taken into consideration. It was discovered that for all structures, the lattice constant of ZnO decreases as the concentration of Ni increases. Furthermore, the calculated structural parameters show a slight departure from Vegard's law, reflecting weak nonlinear alloying effects.

The TB-mBJ-GGA potential was used to evaluate the band gap values, and the band structure and density of states (DOS) analysis verified that the system is semiconducting, with the gap character varying depending on the particular crystal phase. Electronic charge density maps were used to further investigate the bonding nature in $Zn_{1-x}Ni_xO$. These maps showed that pure ZnO has a partially covalent character that progressively decreases with increasing Ni content, enhancing the material's ionic character.

It was discovered that the total magnetic moment increased linearly with Ni content x, reaching 2.0 μ_B per formula unit for NiO in the ZB and RS structures and 4.0 μ_B per formula unit in the WZ structure. A detailed analysis was conducted for optical properties, such as the real and imaginary parts of the dielectric function, refractive index, electron energy loss, reflectivity, and absorption coefficient spectra. When available, the results are in good agreement with the available experimental and theoretical data; otherwise, they are dependable predictions for future use. The RS structure showed the strongest optical absorption of the three phases, indicating that it could be used

in optoelectronic applications. Additionally, it was discovered that all optical spectra were sensitive to changes in the alloy's composition and crystal structure, and this presents encouraging prospects for the development of materials with specialized optical functions.

References

[1] S. Adachi, *Handbook on Physical Properties of Semiconductors*, Vol. 3, 3rd ed. (Springer, US, 2004).

[2] L. Hannachi and N. Bouarissa, Electronic structure and optical properties of $CdSe_xTe_{1-x}$ mixed crystals, Superlattices Microstruct. **44**(6), 794–801 (2008).

[3] A. Gueddim, S. Zerroug, and N. Bouarissa, Optical characteristics of $ZnTe_{1-x}O_x$ alloys from first-principles calculations, J. Lumin. **135**, 243–247 (2013).

[4] D. J. Smith, Atomic-scale characterization of II–VI compound semiconductors, J. Electron. Mater. **42,** 3168–3174 (2013).

[5] V. Tomashyk, P. Feychuk, and L. Shcherbak, *Ternary Alloys Based on II–VI Semiconductor Compounds* (CRC Press Taylor & Francis Group, Boca Raton, 2014).

[6] M. Isshiki and J. Wang, in: *Springer Handbook of Electronic and Photonic Materials*, eds. S. Kasap and P. Capper (Springer, Cham, 2007) pp. 1–18.

[7] K. Kassali and N. Bouarissa, Composition and temperature dependence of electron band structure in $ZnSe_{1-x}S_x$, Mater. Chem. Phys. **76**(3), 255–261 (2002).

[8] H. von Wenckstern, H. Schmidt, M. Brandt, A. Lajn, R. Pickenhain, M. Lorenz, M. Grundmann, D.M. Hofmann, A. Polity, and B.K. Meyer, Anionic and cationic substitution in ZnO, Prog. Solid State Chem. **37**(2–3), 153–172 (2009).

[9] Ü. Özgür, Y.I. Alivov, C. Liu, A. Teke, M.A. Reshchikov, S. Doğan, V. Avrutin, S.-J. Cho, and H. Morkoç, A comprehensive review of ZnO materials and devices, J. Appl. Phys. **98,** 041301 (2005).

[10] B. Bieniek, *Ultra Thin ZnO on Metal Substrates: An ab initio Study*, Ph.D Thesis (Technische Universitaet Berlin, Germany, 2016).

[11] S. Saib and N. Bouarissa, Structural parameters and transition pressures of ZnO: ab-initio calculations, Phys. Status Solidi B **244**(3), 1063–1069 (2007).

[12] T. Dietl, H. Ohno, F. Matsukura, J. Cibert, and D. Ferrand, Zener model description of ferromagnetism in zinc-blende magnetic semiconductors, Science **287**(5455), 1019–1022 (2000).

[13] B.U. Haq, R. Ahmed, A. Afaq, A. Shaari, and M. Zarshenas, Structural and electronic properties of ni-doped ZnO in zinc-blende phase: A DFT investigations, AIP Conf. Proc. **1482**, 54–57 (2012).

[14] B.B. Li, X.Q. Xiu, R. Zhang, Z.K. Tao, L. Chen, Z.L. Xie, and Z. Xie, Study of structure and magnetic properties of Ni-doped ZnO-based DMSs, Mater. Sci. Semicond. Process. **9**(1–3), 141–145 (2006).

[15] T. Dietl, H. Ohno, and F. Matsukura, Hole-mediated ferromagnetism in tetrahedrally coordinated semiconductors, Phys. Rev. B **63**(19), 195205 (2001).

[16] A. Dinia, J.P. Ayoub, G. Schmerber, E. Beaurepaire, D. Muller, and J.J. Grob, Effect of ion irradiation on the structural and the magnetic properties of $Zn_{0.75}Co_{0.25}O$ magnetic semiconductors, Phys. I.ett. A **333**(1–2), 152–156 (2004).

[17] T. Wakano, N. Fujimura, Y. Morinaga, N. Abe, A. Ashida, and T. Ito, Magnetic and magnetotransport properties of ZnO: Ni films, Physica E **10**(1–3), 260–264 (2001).

[18] S.W. Jung, W.I. Park, G.C. Yi, and M.Y. Kim, Fabrication and controlled magnetic properties of Ni/ZnO nanorod heterostructures, Adv. Mater. **15**(16), 1358–1361 (2003).

[19] J.B. Cui and U.J. Gibson, Electrodeposition and room temperature ferromagnetic anisotropy of Co and Ni-doped ZnO nanowire arrays, Appl. Phys. Lett. **87**(13), 133108 (2005).

[20] M. Venkatesan, C.B. Fitzgerald, J.G. Lunney, and J.M.D. Coey, Anisotropic ferromagnetism in substituted zinc oxide, Phys. Rev. Lett. **93**(17), 177206 (2004).

[21] B.B. Li, X.Q. Xiu, R. Zhang, Z.K. Tao, L. Chen, Z.L. Xie, and Z. Xie, Study of structure and magnetic properties of Ni-doped ZnO-based DMSs,

Mater. Sci. Semicond. Process. **9**(1–3), 141–145 (2006).

[22] D.L. Hou, R.B. Zhao, Y.Y. Wei, C.M. Zhen, C.F. Pan, and G.D. Tang, Room temperature ferromagnetism in Ni-doped ZnO films, Curr. Appl. Phys. **10**(1), 124–128 (2010).

[23] B. Pandey, S. Ghosh, P. Srivastava, D.K. Avasthi, D. Kabiraj, and J.C. Pivin, Synthesis and characterization of Ni-doped ZnO: A transparent magnetic semiconductor, J. Magn. Magn. Mater. **320**(24), 3347–3351 (2008).

[24] C.J. Cong, J.H. Hong, Q.Y. Liu, L. Liao, and K.L. Zhang, Synthesis, structure and ferromagnetic properties of Ni-doped ZnO nanoparticles, Solid State Commun. **138**(10–11), 511–515 (2006).

[25] G. Pei, C. Xia, S. Cao, J. Zhang, F. Wu, and J. Xu, Synthesis and magnetic properties of Ni-doped zinc oxide powders, J. Magn. Magn. Mater. **302**(2), 340–342 (2006).

[26] T. Li, H. Qiu, P. Wu, M. Wang, and R. Ma, Characteristics of Ni-doped ZnO: Al films grown on glass by direct current magnetron co-sputtering, Thin Solid Films **515**(7–8), 3905–3909 (2007).

[27] G. Gu, G. Xiang, J. Luo, H. Ren, M. Lan, D. He, and X. Zhang, Magnetism in transition-metal-doped ZnO: A first-principles study, J. Appl. Phys. **112**(2), 023913 (2012).

[28] Z. Jin, T. Fukumura, M. Kawasaki, K. Ando, H. Saito, T. Sekiguchi, and H. Koinuma, High throughput fabrication of transition-metal-doped epitaxial ZnO thin films: A series of oxide-diluted magnetic semiconductors and their properties, Appl. Phys. Lett. **78**(24), 3824–3826 (2001).

[29] Z. Yin, N. Chen, F. Yang, S. Song, C. Chai, J. Zhong, and K. Ibrahim, Structural, magnetic properties and photoemission study of Ni-doped ZnO, Solid State Commun. **135**(7), 430–433 (2005).

[30] G. Pei, C. Xia, B. Wu, T. Wang, L. Zhang, Y. Dong, and J. Xu, Studies of magnetic interactions in Ni-doped ZnO from first-principles calculations, Comput. Mater. Sci. **43**(3), 489–494 (2008).

[31] B.B. Straumal, A.A. Myatiev, P.B. Straumal, A.A. Mazilkin, S.G. Protasova, E. Goering, and B. Baretzky, Grain boundary layers in nanocrystalline ferromagnetic zinc oxide, JETP Lett. **92**(6), 396–400 (2010).

[32] P. Hohenberg and W. Kohn, Inhomogeneous electron gas, Phys. Rev. **136**(3B), B864–B871 (1964).

[33] W. Kohn and L.J. Sham, Self-consistent equations including exchange and correlation effects, Phys. Rev. **140**(4A), A1133–A1138 (1965).

[34] P. Blaha, K. Schwarz, G.K.H. Madsen, D. Kvasnicka, and J. Luitz, *WIEN2k, An Augmented Plane Wave + Local Orbitals Program for Calculating Crystal Properties* (Karlheinz Schwarz, Techn. Universität Wien, Austria, 2008).

[35] F. Tran and P. Blaha, Accurate band gaps of semiconductors and insulators with a semilocal exchange-correlation potential, Phys. Rev. Lett. **102**(22), 226401 (2009).

[36] H.J. Monkhorst and J.D. Pack, Special points for Brillouin-zone integrations, Phys. Rev. B **13**(12), 5188–5192 (1976).

[37] J.D. Pack and H.J. Monkhorst, 'Special points for Brillouin-zone integrations' – A reply, Phys. Rev. B **16**(4), 1748–1749 (1977).

[38] F. Birch, Finite elastic strain of cubic crystals, J. Geophys. Res. **57**, 227 (1952).

[39] Z. Wu and R.E. Cohen, More accurate generalized gradient approximation for solids, Phys. Rev. B **73**(23), 235116 (2006).

[40] B. U. Haq, A. Afaq, R. Ahmed, and S. Naseem, Structural, electronic, and magnetic properties of Co-doped ZnO, Chin. Phys. B **21**(9), 097101 (2012).

[41] B.U. Haq, R. Ahmed, G. Abdellatif, A. Shaari, F.K. Butt, M.B. Kanoun, and S. Goumri-Said, Dominant ferromagnetic coupling over antiferromagnetic in Ni doped ZnO: First-principles calculations, Front. Phys. **11**, 1–7 (2016).

[42] Ü. Özgür, Y.I. Alivov, C. Liu, A. Teke, M.A. Reshchikov, S. Doğan, V. Avrutin, S.-J. Cho, and H. Morkoç, A comprehensive review of ZnO materials and devices, J. Appl. Phys. **98**, 041301 (2005).

[43] H. Benzerouk, F. Chouit, M. Mekhnache, L.S. Hamideche, and A. Drici, An experimental and theoretical study of nickel oxide (NiO) using

the spraying method (CSP) and DFT calculations, Mater. Sci. Eng. B **303**, 117323 (2024).

[44] S. Adachi, *Properties of Group-IV, III–V, and II–VI Semiconductors* (Wiley, Chichester, 2005).

[45] L. Vegard, The constitution of the mixed crystals and the filling of space of the atoms, Z. Phys. **5**, 17–26 (1921).

[46] J. P. Dismukes, L. Ekstrom, and R.J. Paff, Lattice parameter and density in germanium–silicon alloys, J. Phys. Chem. **68**(10), 3021–3027 (1964).

[47] M. Laradji, D.P. Landau, and B. Dünweg, Structural properties of $Si_{1-x}Ge_x$ alloys: A Monte Carlo simulation with the Stillinger-Weber potential, Phys. Rev. B **51**(8), 4894–4904 (1995).

[48] N. Bouarissa, Positron states in $Si_{1-x}Ge_x$ alloys: deviation from Vegard's Law, Mod. Phys. Lett. B **16**(08), 275–283 (2002).

[49] Z. Charifi and N. Bouarissa, The effect of the violation of Vegard's law on the optical bowing in $Si_{1-x}Ge_x$ alloys, Phys. Lett. A **234**(6), 493–497 (1997).

[50] B. Jobst, D. Hommel, U. Lunz, T. Gerhard, and G. Landwehr, E_0 band-gap energy and lattice constant of ternary $Zn_{1-x}Mg_xSe$ as functions of composition, Appl. Phys. Lett. **69**(1), 97–99 (1996).

[51] S. Zerroug, A. Gueddim, M.A. Khan, and N. Bouarissa, *Ab initio* study of structural parameters and optical properties of $ZnTe_{1-x}O_x$, Superlattices Microstruct. **53**, 155–162 (2013).

[52] K. Souleh, A. Amor, H. Ledjici, B. Lagoun, M. Boucenna, and N. Bouarissa, Structural parameters and optical spectra of $Zn_{1-x}Co_xO$ ternary alloys with zinc-blende, rocksalt and wurtzite phases, Optik **224**, 165732 (2020).

[53] S. Zerroug, F. Ali Sahraoui, and N. Bouarissa, *Ab initio* calculations of yttrium nitride: structural and electronic properties, Appl. Phys. A **97**, 345–350 (2009).

[54] F. Benmakhlouf, A. Bechiri, and N. Bouarissa, Zinc-blende ZnS under pressure: predicted electronic properties, Solid-State Electron. **47**(8), 1335–1338 (2003).

[55] K. Kassali and N. Bouarissa, Effect of nitrogen concentration on electronic energy bands of $Ga_{1-x}In_xN_yAs_{1-y}$ alloys, Microelectron. Eng. **54**(3–4), 277–286 (2000).

[56] N. Bouarissa, Electron and positron energy levels and deformation potentials in group-III nitrides, Phys. Status Solidi B **231**(2), 391–402 (2002).

[57] K. Souleh, T. Smain, H. Lidjici, B. Lagoun, M. Boucenna, and N. Bouarissa, Electronic structure and magnetization of $Zn_{1-x}Co_xO$ ternary alloys with zinc-blende, rocksalt and wurtzite phases, Opt. Quantum Electron. **53**(8), 432 (2021).

[58] S.K. Neogi, R. Karmakar, A.K. Misra, A. Banerjee, D. Das, and S. Bandyopadhyay, Physical properties of antiferromagnetic Mn doped ZnO samples: Role of impurity phase, J. Magn. Magn. Mater. **346**, 130–137 (2013).

[59] H. Algarni, A. Gueddim, N. Bouarissa, M.A. Khan, and H. Ziani, Crystal structure and electronic properties of wurtzite $Mg_xZn_{1-x}O$: *Ab initio* study, Results Phys. **15**, 102694 (2019).

[60] S. Zerroug, F. Ali Sahraoui, and N. Bouarissa, Structural parameters and pressure coefficients for CdS_xTe_{1-x}: FP-LAPW calculations, Eur. Phys. J. B **57**, 9–14 (2007).

[61] J.P. Walter and M.L. Cohen, Electronic charge densities in semiconductors, Phys. Rev. Lett. **26**(1), 17–20 (1971).

[62] N. Bouarissa, Electron valence charge densities in $Hg_{1-x}Cd_xTe$ mixed crystals, Infrared Phys. Technol. **39**(5), 265–270 (1998).

[63] S.L. Richardson, M.L. Cohen, S.G. Louie, and J.R. Chelikowsky, Electron charge densities at conduction-band edges of semiconductors, Phys. Rev. B **33**(2), 1177–1180 (1986).

[64] N. Bouarissa and F. Annane, Electronic properties and elastic constants of the ordered $Ge_{1-x}Sn_x$ alloys, Mater. Sci. Eng. B **95**(2), 100–106 (2002).

[65] M.A. Khan and N. Bouarissa, Optical and energy-loss spectra of ZnS from *ab initio* molecular dynamics simulation: temperature effect, Optik **124**(21), 5095–5098 (2013).

[66] N. Bouarissa, The effect of hydrostatic pressure on the electronic and optical properties of InP, Solid State Electron. **44**(12), 2193–2198 (2000).

[67] S. Adachi, *Properties of Semiconductor Alloys: Group-IV, III–V and II–VI Semiconductors* (John Wiley & Sons, Chichester, 2009).

[68] K.I. Suzuki and S. Adachi, Optical constants of $Cd_xZn_{1-x}Se$ ternary alloys, J. Appl. Phys. **83**(2), 1018–1022 (1998).

[69] N. Bouarissa, Energy gaps and refractive indices of $Al_xGa_{1-x}As$, Mater. Chem. Phys. **72**(3), 387–394 (2001).

[70] M. Boucenna and N. Bouarissa, Refractive index and dielectric constants of $Ga_xIn_{1-x}P$: Disorder effect, Optik **125**(22), 6611–6615 (2014).

[71] N.M. Ravindra, P. Ganapathy, and J. Choi, Energy gap–refractive index relations in semiconductors – An overview, Infrared Phys. Technol. **50**(1), 21–29 (2007).

[72] N. Bouarissa, Pressure dependence of refractive index, dielectric constants and optical phonon frequencies of indium arsenide, Optik **138**, 263–268 (2017).

[73] P.Y. Yu and M. Cardona, *Fundamentals of Semiconductors, Physics and Materials Properties* (Springer-Verlag, Berlin, 1996).

[74] A. Gueddim, S. Zerroug, and N. Bouarissa, Optical characteristics of $ZnTe_{1-x}O_x$ alloys from first-principles calculations, J. Lumin. **135**, 243–247 (2013).

MAGNETINIŲ PUSLAIDININKINIŲ LYDINIŲ $Zn_{1-x}Ni_xO$ SFALERITO, AKMENS DRUSKOS IR VURCITO FAZĖSE STRUKTŪRINIŲ, ELEKTRONINIŲ, MAGNETINIŲ IR OPTINIŲ SAVYBIŲ *AB INITIO* TYRIMAS

F. Redjem [a], K. Souleh [b] H. Mouloudj [c], B. Lagoun [d], H. Lidjici [a], S. Djaili [e], A. Amor [f], T. Smain [f]

[a] *Amaro Telidžio universiteto Medžiagų laboratorija atsinaujinančiosios energijos taikymui ir plėtrai, Laguatas, Alžyras*

[b] *Amaro Telidžio universiteto Puslaidininkinių ir dielektrinių medžiagų tyrimo ir kūrimo laboratorija, Laguatas, Alžyras*

[c] *Koubos aukštesniosios normaliosios mokyklos Dalelių fizikos ir statistinės fizikos laboratorija, Alžyras, Alžyras*

[d] *Amaro Telidžio universiteto Medžiagų fizikos ir chemijos laboratorija, Laguatas, Alžyras*

[e] *Laguato mokytojų rengimo mokyklos Fizikos fakultetas, Laguatas, Alžyras*

[f] *Ziano Ašuaro universiteto Fizikos katedra, Dželfa, Alžyras*